Research Square

Preprints are preliminary reports that have not undergone peer review. They should not be considered conclusive, used to inform clinical practice, or referenced by the media as validated information.

Fixed-Time Cooperative Trajectory Tracking Control of Multi-AUV Formation under Unknown Disturbances

Zi-jun HU ZHAO
Shandong Jiaotong University
Yan-cai Yan-cai
yancaihu@126.com

Shandong Jiaotong University
Sheng-da LI DING
Shandong Jiaotong University
Xin-yi Wei-hong LI
Shandong Jiaotong University

Research Article

Keywords: autonomous underwater vehicle, formation control, sliding mode control, fixed-time control, disturbance observer

Posted Date: September 22nd, 2026

DOI: https://doi.org/10.21203/rs.3.rs-11074032/v1

License: This work is licensed under a Creative Commons Attribution 4.0 International License. Read Full License

Additional Declarations: No competing interests reported.

Fixed-Time Cooperative Trajectory Tracking Control of Multi-AUV Formation under Unknown Disturbances

ZHAO Zi-jun, HU Yan-cai✉, DING Sheng-da, LI Wei-hong, LI Xin-yi

(*School of Navigation and Shipping*, Shandong Jiaotong University, Weihai 264200, China)

Abstract : To address the degradation of trajectory tracking accuracy for multi-AUV formations caused by unknown environmental disturbances and the slow convergence drawback of traditional control strategies, this paper proposes a fixed-time cooperative trajectory tracking control scheme based on a disturbance observer. Firstly, a kinematic and dynamic two-layer model with disturbances is established, and a fixed-time disturbance observer (FTDO) is designed to rapidly and accurately estimate unknown disturbances. Secondly, a control law is developed by integrating sliding mode with observer feedforward compensation, which can effectively counteract disturbances and suppress system chattering simultaneously. In terms of formation cooperation, the leader-follower method combined with geometric constraints is adopted to construct the formation control law, ensuring efficient coordination of multiple AUVs and complex trajectory tracking. Lyapunov theory is employed to strictly prove that all system errors can converge within a fixed time independent of initial states. Finally, simulations of multi-configuration formations and complex paths verify that the proposed scheme possesses superior tracking accuracy and robustness under arbitrary initial configurations and unknown disturbances.

Keywords : autonomous underwater vehicle; formation control; sliding mode control; fixed-time control; disturbance observer

1 Introduction

As one of the most important strategic spaces on Earth, the ocean holds profound significance for sustainable human development through resource exploitation and environmental monitoring. Autonomous Underwater Vehicles (AUVs), with their high autonomy and flexibility, have become core tools for underwater search, resource exploration, and scientific investigation. However, single AUVs have inherent limitations in terms of energy endurance, operational efficiency, and fault tolerance. To meet the increasing demands of complex deep-sea operations, multi-AUV formation control technology has become a research focus in the field of marine robotics. Through cooperative coordination among multiple AUVs, wider area coverage and higher task redundancy can be achieved (An et al., 2022).

In the development of AUV formation control, traditional linear feedback control has been widely used but relies heavily on accurate linearized mathematical models. Due to the strongly nonlinear characteristics of underwater environments, simple feedback mechanisms often struggle to maintain stable formation configurations in highly time-varying flow fields (Bravo et al., 2025). To enhance system robustness, researchers have introduced sliding mode control (SMC) technology. SMC offers excellent immunity to model parameter uncertainties and external disturbances, effectively handling the nonlinear coupling in AUV dynamics (Li et al., 2022). Hossein et al. (2018) designed a consensus-based sliding mode control scheme for formation tracking problems in multi-agent systems. However, traditional SMC typically exhibits asymptotic convergence,

Fund Project: Shandong Provincial Higher Education Youth Innovation Team Program (2022KJ210), Shandong Provincial Key Research and Development Program (Major Scientific and Technological Innovation Project 2024CXGC010804)

Author Biographies: Zhao Zijun, male, master's student, research interests: nonlinear control, ship course control.

Ding Shengda, male, master's student, research interests: nonlinear control, ship course control.

Li Weihong, male, master's student, research interests: nonlinear control, ship course control.

Li Xinyi, female, master's student, research interests: nonlinear control, ship course control.

Corresponding Author: Hu Yancai, male, associate professor, Ph.D., research interests: ship collision avoidance, ship motion control, (E-mail: yancaihu@126.com).

meaning system states only reach equilibrium as time approaches infinity, which is insufficient for underwater operations requiring high real-time performance (Alireza et al., 2022; Liu et al., 2022).

To achieve faster response, finite-time control theory has been deeply investigated. Unlike asymptotic convergence, finite-time control ensures system states converge to equilibrium within a finite time (Xu et al., 2019). Shou et al. (2022) discussed finite-time formation control and obstacle avoidance for multi-agent systems, incorporating finite-time theory to enhance dynamic response. However, in practice, the upper bound of convergence time for finite-time control strictly depends on the system's initial states. If the initial deviation is too large, convergence time increases significantly, limiting its application in AUV deployment tasks where initial positions are unknown (Zhou et al., 2021).

To address this limitation, fixed-time control technology has emerged. Its core advantage is that the upper bound of convergence time is independent of the system's initial states and is determined only by controller parameters (Liu et al., 2022;Cui et al., 2025). Wang et al. (2025) proposed a fixed-time control strategy for uncertain nonlinear systems to solve consensus problems among agents. Su et al. (2021) further investigated event-triggered fixed-time formation control for underwater vehicles to reduce communication energy consumption. However, existing fixed-time studies often neglect refined disturbance compensation when dealing with extremely complex underwater dynamics (Zhang et al., 2025). AUVs operating in real-world conditions suffer from long-term exposure to unknown ocean currents and external noise, which are highly stochastic and difficult to model directly. Although sliding mode control can suppress disturbances by increasing switching gains, excessive gain leads to severe control chattering, damaging underwater thrusters (Jin et al., 2026). Therefore, designing an efficient disturbance observer has become critical for improving tracking accuracy. However, traditional observers typically achieve only asymptotic estimation, and within the fixed-time control framework, the observer's convergence rate must match the control law; otherwise, overall system stability is affected (An et al., 2023).

In summary, to meet the high-precision formation control requirements of multi-AUV systems under unknown disturbances, this paper designs a robust control scheme with fixed-time convergence characteristics. First, a fixed-time disturbance observer (FTDO) is developed to achieve fast and accurate estimation of unknown environmental disturbances, overcoming the slow convergence of traditional observers. Second, a fixed-time sliding mode control (FTSMC) law is designed using sliding mode techniques, where the observer's estimated values are used for feedforward compensation, effectively canceling disturbances without increasing gains. For formation coordination, the leader–follower approach combined with geometric constraints achieves efficient multi-vehicle cooperation. Compared with existing studies, this paper uses phased Lyapunov stability proofs to ensure that all system states converge to zero or its neighborhood within fixed time, significantly improving formation accuracy and robustness in complex underwater environments.

The main contributions of this paper are as follows:

1) Existing multi-AUV cooperative control studies (Zhang et al., 2025)typically treat underwater environmental flow disturbances, unmodeled dynamics, and parameter perturbations as a lumped disturbance. This paper constructs a dual-layer model considering disturbances at both the kinematic and dynamic layers. This layered compensation strategy avoids the strong nonlinear coupling introduced by lumped treatment, effectively reducing the complexity of multivariable control design.

2) Traditional disturbance observers suffer from slow convergence and difficulty adapting to rapidly time-varying deep-sea flow fields; finite-time observers have convergence times dependent on initial system states (Xu et al., 2019). To address this, this paper designs a fixed-time disturbance observer and rigorously proves, through phased Lyapunov analysis, that its estimation error converges to zero within fixed time. The upper bound of the observer's convergence time is independent of initial estimation errors, ensuring that the multi-AUV system can achieve fast and accurate estimation of time-varying ocean current disturbances under arbitrary initial deployment conditions.

3) This paper combines sliding mode control with feedforward compensation based on a fixed-time disturbance observer (FTDO) to design a fixed-time formation control law under angle-distance geometric constraints. By introducing a fractional power reaching law and incorporating the leader's real-time dynamics, the proposed method enables

multi-AUV formations to maintain high tracking accuracy even under complex trajectories such as triangular circles and polygonal composites. Moreover, it significantly reduces high-frequency chattering, achieving a balance between control input smoothness and response speed.

2 AUV System Modeling and Prerequisite Knowledge

2.1. AUV Kinematics and Dynamics Model

Autonomous Underwater Vehicles (AUVs) are a subset of mobile robot systems. A schematic diagram of an AUV is shown in Figure 1. To describe the system motion, we use two coordinate frames: a fixed coordinate frame (inertial frame) and a moving coordinate frame (with its origin at the AUV's center of gravity). In this paper, only the horizontal motion of the AUV is considered, while roll and pitch motions are neglected.

Define the position and orientation in the inertial coordinate system as $\boldsymbol{\eta}=[x,y,\psi]^{\boldsymbol{T}}$,Velocity in the body-fixed coordinate system is $\boldsymbol{v}=[u,v,r]^{\boldsymbol{T}}$.

The kinematic model and kinematic model of the AUV are described as (Repoulias et al., 2007) :

$$\dot{\boldsymbol{\eta}}=\boldsymbol{R}(\psi)\boldsymbol{v} \tag{1}$$

$$\boldsymbol{M}\dot{\boldsymbol{v}}+\boldsymbol{C}(\boldsymbol{v})\boldsymbol{v}+\boldsymbol{D}(\boldsymbol{v})\boldsymbol{v}=\boldsymbol{\tau}+\boldsymbol{\tau}_d \tag{2}$$

Among them, $\mathbf{R}(\psi)$ for the transformation matrix.

$$\mathbf{R}(\psi)=\begin{bmatrix}\cos\psi & -\sin\psi & 0\\ \sin\psi & \cos\psi & 0\\ 0 & 0 & 1\end{bmatrix} \tag{3}$$

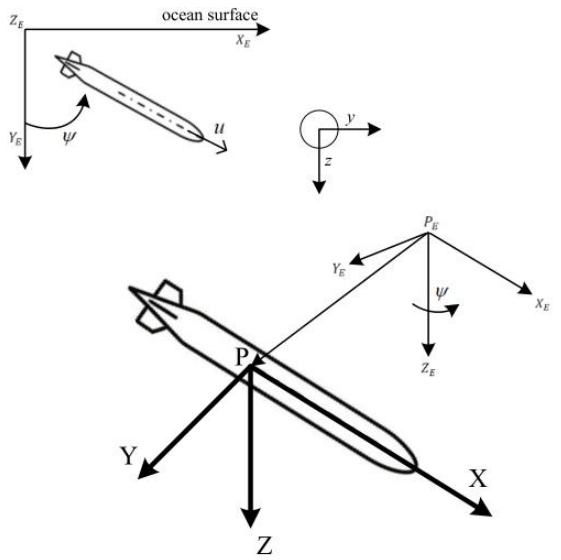

Fig. 1. The AUV in motion plane

Among them, $\boldsymbol{\tau}=[\tau_u,\tau_v,\tau_r]^T$ as the control input, $\boldsymbol{\tau}_d=[d_u,d_v,d_r]^T$ is the lumped unknown external disturbance and model parameter perturbation. inertia matrix $\boldsymbol{M}$ 、Coriolis and centripetal force matrix $\boldsymbol{C}(\boldsymbol{v})$ 、hydrodynamic damping matrix $\boldsymbol{D}(\boldsymbol{v})$ are respectively：

$$\boldsymbol{M}=\mathrm{diag}(m_{11},m_{22},m_{33}) \tag{4}$$

$$\boldsymbol{C}(\boldsymbol{v})=\begin{bmatrix}0 & 0 & -m_{22}v\\ 0 & 0 & m_{11}u\\ m_{22}v & -m_{11}u & 0\end{bmatrix} \tag{5}$$

$$\boldsymbol{D}(\boldsymbol{v})=\mathrm{diag}(X_u+X_{u|u|}|u|,Y_v+Y_{v|v|}|v|,N_r+N_{r|r|}|r|) \tag{6}$$

To facilitate the observer design, Equation (2) is rewritten into a standard form：

$$\dot{\boldsymbol{v}}=\boldsymbol{f}(\boldsymbol{v})+\boldsymbol{M}^{-1}\boldsymbol{\tau}+\boldsymbol{d}(t) \tag{7}$$

where the nonlinear term is $\boldsymbol{f}(\boldsymbol{v})=-\boldsymbol{M}^{-1}[\boldsymbol{C}(\boldsymbol{v})\boldsymbol{v}+\boldsymbol{D}(\boldsymbol{v})\boldsymbol{v}]$, where the equivalent lumped disturbance is $\boldsymbol{d}(t)=\boldsymbol{M}^{-1}\boldsymbol{\tau}_d$.

2.2. Preliminary Theorems and Assumptions

To ensure the rigor of the formula derivation, the following assumptions, definitions, and lemmas are introduced. For simplicity of writing, for a constant $\gamma>0$ and a vector $\boldsymbol{x}=[x_1,x_2,\ldots,x_n]^T$, $\lfloor \boldsymbol{x}\rfloor^{\gamma}=[|x_1|^{\gamma}\,\mathrm{sgn}(x_1),\ldots,|x_n|^{\gamma}\,\mathrm{sgn}(x_n)]^T$ is defined.In the fixed-time control framework, the operator $sig^{a}(\cdot)$ in the observer design is used to achieve fixed-time convergence.

Assumption 1: The equivalent lumped disturbance $\boldsymbol{d}(t)$ and its first derivative are both bounded; that is, there exists a positive constant L_1,L_2 such that:

$$\| \boldsymbol{d}(t)\| \le L_1 \tag{8}$$

$$\|\dot{\boldsymbol{d}}(t)\| \le L_2 \tag{9}$$

Lemma 1 (Jiang et al., 2016): Consider the nonlinear system $\dot{\boldsymbol{x}} = f(\boldsymbol{x},t)$. If there exist a continuous positive definite function $V(\boldsymbol{x})$ and a scalar $\alpha > 0, \beta > 0, p \in (0,1), q > 1$ such that:

$$\dot{V}(\boldsymbol{x}) \le -\alpha V^p(\boldsymbol{x}) - \beta V^q(\boldsymbol{x}) \tag{10}$$

Then the origin of the system is globally fixed-time stable, and the settling time T is bounded, satisfying:

$$T \le T_{max} = \frac{1}{\alpha(1-p)} + \frac{1}{\beta(q-1)} \tag{11}$$

Lemma 2 (Polyakov et al., 2012; Behera et al., 2016): If there exists a positive definite function $V(\boldsymbol{x})$ satisfying $\dot{V}(\boldsymbol{x}) \le -\alpha V^p(\boldsymbol{x}) - \beta V^q(\boldsymbol{x}) + \Delta$, where $\Delta > 0$, then the system trajectory can converge to a residual set of the origin within a fixed time, and its practical settling time bound is given by $T \le \frac{1}{\alpha(1-p)\theta} + \frac{1}{\beta(q-1)\theta}$, where $0 < \theta < 1$.

3 Controller Design

3.1. Construct a fixed-time disturbance observer

Remark 1: Observing the structure of the observer designed in Equations (12)-(13), it can be found that the introduction of the constant power terms α_1 and β_1 is the key to breaking the traditional asymptotic convergence limitation and achieving fixed-time stability. Specifically, when the estimation error is large ($\| e_v \| > 1$), the high-order nonlinear term $\mathrm{sig}^{\alpha_1}(e_v)$ plays a dominant role, providing a superlinear strong error-correction driving force that accelerates the system state toward the equilibrium point. When the system approaches the equilibrium point ($\| e_v \| < 1$), the fractional-order term $\mathrm{sig}^{\beta_1}(e_v)$ takes over the dominance, ensuring that the system maintains a nonzero convergence slope within the residual neighborhood, thereby eliminating the drawback of slow tail convergence inherent in traditional linear observers.

To accurately estimate the unknown disturbance $\boldsymbol{d}(t)$ in the nonlinear model within a fixed time, the following fixed-time disturbance observer is designed:

$$\dot{\hat{\boldsymbol{v}}} = \boldsymbol{f}(\boldsymbol{v}) + \boldsymbol{M}^{-1}\boldsymbol{\tau} + \boldsymbol{d} + \boldsymbol{\Lambda}_1 \lfloor \boldsymbol{e}_v \rfloor^{\alpha_1} + \boldsymbol{\Lambda}_2 \lfloor \boldsymbol{e}_v \rfloor^{\beta_1} \tag{12}$$

$$\dot{\boldsymbol{d}} = \boldsymbol{\Lambda}_3 \lfloor \boldsymbol{e}_v \rfloor^{2\alpha_1 - 1} + \boldsymbol{\Lambda}_4 \lfloor \boldsymbol{e}_v \rfloor^{2\beta_1 - 1} + \boldsymbol{\Lambda}_5 \mathrm{sgn}(\boldsymbol{e}_v) \tag{13}$$

Where $\hat{\boldsymbol{v}}$ and $\boldsymbol{d}$ are the estimates of the system velocity and the disturbance, respectively. The velocity estimation error is defined as $\boldsymbol{e}_v = \boldsymbol{v} - \hat{\boldsymbol{v}}$, and the disturbance estimation error is defined as $\boldsymbol{e}_d = \boldsymbol{d} - \boldsymbol{d}$. $\boldsymbol{\Lambda}_i (i = 1..5)$ is a positive definite diagonal gain matrix, and $\alpha_1 \in (0.5,1)$, $\beta_1 > 1$ is a constant.

Combining Equation (7) with Equations (12)-(13), the error dynamics of the observer can be obtained as:

$$\dot{\boldsymbol{e}}_v = \boldsymbol{e}_d - \boldsymbol{\Lambda}_1 \lfloor \boldsymbol{e}_v \rfloor^{\alpha_1} - \boldsymbol{\Lambda}_2 \lfloor \boldsymbol{e}_v \rfloor^{\beta_1} \tag{14}$$

$$\dot{\boldsymbol{e}}_d = \dot{\boldsymbol{d}} - \boldsymbol{\Lambda}_3 \lfloor \boldsymbol{e}_v \rfloor^{2\alpha_1 - 1} - \boldsymbol{\Lambda}_4 \lfloor \boldsymbol{e}_v \rfloor^{2\beta_1 - 1} - \boldsymbol{\Lambda}_5 \mathrm{sgn}(\boldsymbol{e}_v) \tag{15}$$

3.2. Stability proof of the fixed-time disturbance observer

Theorem 1: Based on Assumption 1, by appropriately selecting the observer gain matrix $\boldsymbol{\Lambda}_i$, the observer error system (14)-(15) can converge to zero within a fixed time T_{obs}, i.e., achieving accurate disturbance estimation $\boldsymbol{d} \to \boldsymbol{d}$.

Construct the Lyapunov function as:

$$V_{obs} = \frac{1}{2}\boldsymbol{e}_v^T \boldsymbol{e}_v + \frac{1}{2}\boldsymbol{e}_d^T \boldsymbol{\Lambda}_3^{-1} \boldsymbol{e}_d \tag{16}$$

Taking the derivative of V_{obs} and substituting the error dynamics yields:

$$\dot{V}_{obs} = \boldsymbol{e}_v^T \dot{\boldsymbol{e}}_v + \boldsymbol{e}_d^T \boldsymbol{\Lambda}_3^{-1} \dot{\boldsymbol{e}}_d \tag{17}$$

$$\begin{aligned} \dot{V}_{obs} &= \boldsymbol{e}_v^T (\boldsymbol{e}_d - \boldsymbol{\Lambda}_1 \lfloor \boldsymbol{e}_v \rfloor^{\alpha_1} - \boldsymbol{\Lambda}_2 \lfloor \boldsymbol{e}_v \rfloor^{\beta_1}) \\ &+ \boldsymbol{e}_d^T \boldsymbol{\Lambda}_3^{-1} (\dot{\boldsymbol{d}} - \boldsymbol{\Lambda}_3 \lfloor \boldsymbol{e}_v \rfloor^{2\alpha_1 - 1} - \boldsymbol{\Lambda}_4 \lfloor \boldsymbol{e}_v \rfloor^{2\beta_1 - 1} - \boldsymbol{\Lambda}_5 \mathrm{sgn}(\boldsymbol{e}_v)) \end{aligned} \tag{18}$$

By selecting a sufficiently large gain matrix such that the dominant term satisfies $\dot{V}_{obs} \le -c_1 V_{obs}^{\gamma_1} - c_2 V_{obs}^{\gamma_2}$, it follows from Lemma 1 that the observation error will converge within a fixed time T_{obs}.

3.3. Design of fixed-time sliding mode control law

The control system is structured as a cascade of a kinematic loop and a dynamic loop. The reference trajectory of the AUV is defined as $\eta_d = [x_d, y_d, \psi_d]^T$.

Step 1: Design of the kinematic virtual control law:

Define the position tracking error as $\boldsymbol{e}_1$:

$$\boldsymbol{e}_1 = \boldsymbol{\eta} - \boldsymbol{\eta}_d \tag{19}$$

Taking its derivative yields the position error dynamics:

$$\dot{\boldsymbol{e}}_1 = \boldsymbol{R}(\psi)\boldsymbol{v} - \dot{\boldsymbol{\eta}}_d \tag{20}$$

To make $\boldsymbol{e}_1$ converge within a fixed time, the fixed-time kinematic virtual control law $\boldsymbol{\alpha}_v$ is designed as: :

$$\boldsymbol{\alpha}_v = \boldsymbol{R}^{-1}(\psi)\left[\dot{\boldsymbol{\eta}}_d - \boldsymbol{K}_1\lfloor \boldsymbol{e}_1 \rfloor^{p_1} - \boldsymbol{K}_2\lfloor \boldsymbol{e}_1 \rfloor^{q_1}\right] \tag{21}$$

where $\boldsymbol{K}_1, \boldsymbol{K}_2$ is a positive definite diagonal gain matrix, $0 < p_1 < 1, q_1 > 1$.

If the velocity error $\boldsymbol{e}_2 = \boldsymbol{v} - \boldsymbol{\alpha}_v$ is defined, substituting it into Equation (20) yields:

$$\begin{aligned} \dot{\boldsymbol{e}}_1 &= \boldsymbol{R}(\psi)(\boldsymbol{e}_2 + \boldsymbol{\alpha}_v) - \dot{\boldsymbol{\eta}}_d \\ &= \boldsymbol{R}(\psi)\boldsymbol{e}_2 - \boldsymbol{K}_1\lfloor \boldsymbol{e}_1 \rfloor^{p_1} - \boldsymbol{K}_2\lfloor \boldsymbol{e}_1 \rfloor^{q_1} \end{aligned} \tag{22}$$

Step 2: Design of the dynamic control law:

Compute the derivative of the virtual control law to obtain the desired acceleration:

$$\begin{aligned} \dot{\boldsymbol{\alpha}}_v &= \dot{\boldsymbol{R}}^{-1}(\psi)\left[\dot{\boldsymbol{\eta}}_d - \boldsymbol{K}_1\lfloor \boldsymbol{e}_1 \rfloor^{p_1} - \boldsymbol{K}_2\lfloor \boldsymbol{e}_1 \rfloor^{q_1}\right] + \\ &\boldsymbol{R}^{-1}(\psi)\left[\ddot{\boldsymbol{\eta}}_d - \boldsymbol{K}_1 p_1 |\boldsymbol{e}_1|^{p_1-1}\dot{\boldsymbol{e}}_1 - \boldsymbol{K}_2 q_1 |\boldsymbol{e}_1|^{q_1-1}\dot{\boldsymbol{e}}_1\right] \end{aligned} \tag{23}$$

Design the fixed-time sliding surface $\boldsymbol{S}$:

$$\boldsymbol{S} = \boldsymbol{e}_2 + \int_0^t \left(\boldsymbol{C}_1\lfloor \boldsymbol{e}_2 \rfloor^{p_2} + \boldsymbol{C}_2\lfloor \boldsymbol{e}_2 \rfloor^{q_2}\right)d\tau \tag{24}$$

Among them, $\boldsymbol{C}_1, \boldsymbol{C}_2 > 0$ is a diagonal matrix, $0 < p_2 < 1, q_2 > 1$.

Taking the derivative of the sliding surface yields:

$$\dot{\boldsymbol{S}} = \dot{\boldsymbol{e}}_2 + \boldsymbol{C}_1\lfloor \boldsymbol{e}_2 \rfloor^{p_2} + \boldsymbol{C}_2\lfloor \boldsymbol{e}_2 \rfloor^{q_2} \tag{25}$$

Substituting $\dot{\boldsymbol{e}}_2 = \dot{\boldsymbol{v}} - \dot{\boldsymbol{\alpha}}_v$ into Equation (25) and combining with the system dynamic equation (7) yields:

$$\dot{\boldsymbol{S}} = \boldsymbol{f}(\boldsymbol{v}) + \boldsymbol{M}^{-1}\boldsymbol{\tau} + \boldsymbol{d}(t) - \dot{\boldsymbol{\alpha}}_v + \boldsymbol{C}_1\lfloor \boldsymbol{e}_2 \rfloor^{p_2} + \boldsymbol{C}_2\lfloor \boldsymbol{e}_2 \rfloor^{q_2} \tag{26}$$

Combining the disturbance estimate $\boldsymbol{d}$ provided by the fixed-time disturbance observer, the composite dynamic control law $\boldsymbol{\tau}$ is designed as:

$$\boldsymbol{\tau} = \boldsymbol{M}\left[-\boldsymbol{f}(\boldsymbol{v}) - \boldsymbol{d} + \dot{\boldsymbol{\alpha}}_v - \boldsymbol{C}_1\lfloor \boldsymbol{e}_2 \rfloor^{p_2} - \boldsymbol{C}_2\lfloor \boldsymbol{e}_2 \rfloor^{q_2} - \boldsymbol{K}_3\lfloor \boldsymbol{S} \rfloor^{p_3} - \boldsymbol{K}_4\lfloor \boldsymbol{S} \rfloor^{q_3}\right] \tag{27}$$

where $\boldsymbol{K}_3, \boldsymbol{K}_4$ is a positive definite diagonal matrix, and $0 < p_3 < 1, q_3 > 1$. The last term employs a fractional-power reaching law, which can drive the system state to the sliding surface within a fixed time and effectively avoid the severe chattering caused by traditional sign functions.

Remark 2: The dynamic control law (27) designed in this paper consists of three parts: the equivalent control term, the FTDO disturbance feedforward compensation term $\boldsymbol{d}$, and the fixed-time sliding mode reaching term. Traditional sliding mode controllers [3] lack robust estimation of ocean current disturbances and therefore must set the gain of the sign function in the reaching law to be larger than the maximum upper bound of the external disturbance. This "strong against strong" approach is the root cause of severe thruster chattering and the induction of nonlinear limit cycles (as shown by the ASMC method in the simulation comparison). In contrast, the proposed scheme feeds the real-time estimated value $\boldsymbol{d}$ from the observer forward into the control law, enabling the controller to actively cancel most of the unknown ocean currents and model perturbations.

Substituting the control law (27) into Equation (26), the closed-loop sliding mode dynamics are obtained as:

$$\dot{\boldsymbol{S}} = \boldsymbol{e}_d - \boldsymbol{K}_3\lfloor \boldsymbol{S} \rfloor^{p_3} - \boldsymbol{K}_4\lfloor \boldsymbol{S} \rfloor^{q_3} \tag{28}$$

After the observer converges within the fixed time T_{obs} , $\boldsymbol{e}_d = 0$, The above equation becomes:

$$\dot{\boldsymbol{S}} = -\boldsymbol{K}_3\lfloor \boldsymbol{S} \rfloor^{p_3} - \boldsymbol{K}_4\lfloor \boldsymbol{S} \rfloor^{q_3} \tag{29}$$

3.4. Fixed-Time Sliding Mode Control Law Stability Proof

Theorem 2: Under the action of the control law (27) and the observer (12)-(13), the trajectory tracking error $\boldsymbol{e}_1$ and the velocity tracking error $\boldsymbol{e}_2$ of the AUV system will asymptotically converge to zero within a fixed time T_{total} .

Define the Lyapunov function for the overall closed-loop system as:

$$V_c = \frac{1}{2}\boldsymbol{e}_1^T\boldsymbol{e}_1 + \frac{1}{2}\boldsymbol{S}^T\boldsymbol{S} \tag{30}$$

Taking its time derivative and substituting into Equations (22) and (29) (assuming $t > T_{obs}$, the disturbance has been compensated for):

$$\dot{V}_c = \boldsymbol{e}_1^T\dot{\boldsymbol{e}}_1 + \boldsymbol{S}^T\dot{\boldsymbol{S}} \tag{31}$$

$$\begin{aligned} \dot{V}_c &= \boldsymbol{e}_1^T\left[\boldsymbol{R}(\psi)\boldsymbol{e}_2 - \boldsymbol{K}_1\lfloor \boldsymbol{e}_1 \rfloor^{p_1} - \boldsymbol{K}_2\lfloor \boldsymbol{e}_1 \rfloor^{q_1}\right] \\ &+ \boldsymbol{S}^T\left[-\boldsymbol{K}_3\lfloor \boldsymbol{S} \rfloor^{p_3} - \boldsymbol{K}_4\lfloor \boldsymbol{S} \rfloor^{q_3}\right] \end{aligned} \tag{32}$$

Unfolded:

$$\dot{V}_c = \boldsymbol{e}_1^T \boldsymbol{R}(\psi)\boldsymbol{e}_2 - \boldsymbol{e}_1^T \boldsymbol{K}_1 \lfloor \boldsymbol{e}_1 \rfloor^{p_1} - \boldsymbol{e}_1^T \boldsymbol{K}_2 \lfloor \boldsymbol{e}_1 \rfloor^{q_1} - \boldsymbol{S}^T \boldsymbol{K}_3 \lfloor \boldsymbol{S} \rfloor^{p_3} - \boldsymbol{S}^T \boldsymbol{K}_4 \lfloor \boldsymbol{S} \rfloor^{q_3} \tag{33}$$

After $\boldsymbol{S}$ converges to 0, it follows from Equation (24) that $\boldsymbol{e}_2$ converges to 0 along the sliding surface. Considering the behavior of the system after reaching the sliding surface ($\boldsymbol{e}_2 \to 0$), and the cross term $\boldsymbol{e}_1^T \boldsymbol{R}(\psi)\boldsymbol{e}_2 \to 0$, we have :

$$\dot{V}_c \le -\lambda_{min}(\boldsymbol{K}_1)\| \boldsymbol{e}_1\|^{p_1+1} - \lambda_{min}(\boldsymbol{K}_2)\| \boldsymbol{e}_1\|^{q_1+1} - \lambda_{min}(\boldsymbol{K}_3)\| \boldsymbol{S}\|^{p_3+1} - \lambda_{min}(\boldsymbol{K}_4)\| \boldsymbol{S}\|^{q_3+1} \tag{34}$$

Using algebraic properties such as inequality $(\sum z_i)^a \le \sum z_i^a$, the above expression can be rewritten into a standard fixed-time stability form as:

$$\dot{V}_c \le -a_1 V_c^{\gamma_1} - a_2 V_c^{\gamma_2} \tag{35}$$

where , $\gamma_1 = \min(\frac{p_1+1}{2}, \frac{p_3+1}{2}) \in (0.5,1)$, $\gamma_2 = \min(\frac{q_1+1}{2}, \frac{q_3+1}{2}) > 1$. According to Lemma 1, the control system is globally fixed-time stable, with the total settling time $T_{total} \le T_{obs} + T_s + T_e$, which ensures the robust convergence of the system.

4 Formation control

This section introduces the AUV formation control algorithm. The proposed geometric model uses laser sensors to measure relative positions. By employing the angle-distance geometry l_{ix}, l_{iy}, Based on this, to determine the desired position of each robot within the group, it is only necessary to specify its distance from the leader and the horizontal angle of the line connecting them. The follower i tracks the leader to achieve the desired distance and desired angle l_{di}, ϕ_{di}. Assuming point P is the reference point, according to Figure 2, with the configuration variable $\eta_{di} = [x_{di}, y_{di}, \psi_{di}]^T$ of followers i, Aimed at following with pose variables $\eta_L = [x_L, y_L, \psi_L]^T$ of Leader。To maintain a specific formation geometry, the desired position of follower i relative to the leader C is determined by the configuration vector $l_i = [l_{ix}, l_{iy}]^T$.

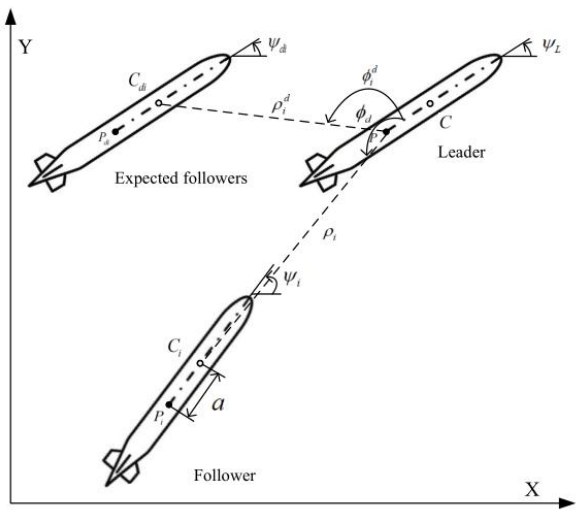

Fig.2. AUV Formation Control

4.1. Formation error modeling

The pose of follower i in the inertial coordinate system is $[x_{di}, y_{di}, \psi_{di}]^T$, which depends on the pose of the leader and the relative formation requirements:

$$x_{di} = x_L + l_{ix}\cos(\phi_d + \psi_L) - l_{iy}\cos\psi_{di} \tag{36}$$

$$y_{di} = y_L + l_{ix}\sin(\phi_d + \psi_L) - l_{iy}\sin\psi_{di} \tag{37}$$

$$\psi_{di} = \psi_{di} \tag{38}$$

The desired pose of follower i in the inertial coordinate system is $[x_i, y_i, \phi_{di}]^T$:

$$x_i = x_L + l_{di}\cos(\phi_{di} + \psi_L) - l_{iy}\cos\psi_{di} \tag{39}$$

$$y_i = y_L + l_{di}\sin(\phi_{di} + \psi_L) - l_{iy}\sin\psi_{di} \tag{40}$$

$$\phi_{di} = \psi_L \tag{41}$$

Define the position error in the inertial coordinate system as:

$$\boldsymbol{e}_{Ii} = \begin{bmatrix} e_{xi} \\ e_{yi} \\ e_{\psi i} \end{bmatrix} = \begin{bmatrix} x_i - x_{di} \\ y_i - y_{di} \\ \phi_{di} - \psi_{di} \end{bmatrix} \tag{42}$$

To implement control using the velocities in the body coordinate system, it is transformed into the body-fixed coordinate system of the i-th follower:

$$\boldsymbol{e}_{Fi} = \begin{bmatrix} e_{ui} \\ e_{vi} \\ e_{ri} \end{bmatrix} = \boldsymbol{R}^T(\psi_i)\boldsymbol{e}_{Ii} \tag{43}$$

Taking the derivative of the above expression yields the formation kinematic error dynamics:

$$\dot{\boldsymbol{e}}_{Fi} = \dot{\boldsymbol{R}}^T(\psi_i)\boldsymbol{e}_{Ii} + \boldsymbol{R}^T(\psi_i)\dot{\boldsymbol{e}}_{Ii} \tag{44}$$

Known $\dot{\boldsymbol{R}}^T(\psi_i) = -r_i \boldsymbol{S}_k \boldsymbol{R}^T(\psi_i)$, among them $\boldsymbol{S}_k = [0,-1,0;1,0,0;0,0,0]$. Substituting into equation (1) gives:

$$\dot{\boldsymbol{e}}_{Fi} = -r_i \boldsymbol{S}_k \boldsymbol{e}_{Fi} + \boldsymbol{v}_i - \boldsymbol{R}^T(\psi_i)\dot{\boldsymbol{\eta}}_{di} \tag{45}$$

4.2. Design and verification of fixed-time sliding mode control for formation

Considering Equation (45) as a new kinematic state equation, to achieve the formation error $\boldsymbol{e}_{Fi} \to 0$,the formation virtual velocity command $\boldsymbol{\alpha}_{Fi}$ is designed as:

$$\begin{aligned}\boldsymbol{\alpha}_{Fi} &= \boldsymbol{R}^T(\psi_i)\dot{\boldsymbol{\eta}}_{di} + r_i \boldsymbol{S}_k \boldsymbol{e}_{Fi} \\ &\quad -\boldsymbol{\Gamma}_1 \lfloor \boldsymbol{e}_{Fi} \rfloor^{\gamma_1} - \boldsymbol{\Gamma}_2 \lfloor \boldsymbol{e}_{Fi} \rfloor^{\gamma_2}\end{aligned} \tag{46}$$

Where $\boldsymbol{\Gamma}_1, \boldsymbol{\Gamma}_2$ is a positive definite diagonal matrix, $\gamma_1 \in (0,1), \gamma_2 > 1$.

Define the velocity error of follower i as:

$$\boldsymbol{e}_{2i} = \boldsymbol{v}_i - \boldsymbol{\alpha}_{Fi} \tag{47}$$

Design the fixed-time sliding surface for formation as:

$$\boldsymbol{S}_{Fi} = \boldsymbol{e}_{2i} + \int_0^t \left(\boldsymbol{C}_{F1} \lfloor \boldsymbol{e}_{2i} \rfloor^{\mu_1} + \boldsymbol{C}_{F2} \lfloor \boldsymbol{e}_{2i} \rfloor^{\mu_2} \right) d\tau \tag{48}$$

Taking the derivative yields:

$$\dot{\boldsymbol{S}}_{Fi} = \dot{\boldsymbol{v}}_i - \dot{\boldsymbol{\alpha}}_{Fi} + \boldsymbol{C}_{F1} \lfloor \boldsymbol{e}_{2i} \rfloor^{\mu_1} + \boldsymbol{C}_{F2} \lfloor \boldsymbol{e}_{2i} \rfloor^{\mu_2} \tag{49}$$

$$\begin{aligned}\dot{\boldsymbol{S}}_{Fi} &= \boldsymbol{f}(\boldsymbol{v}_i) + \boldsymbol{M}^{-1}\boldsymbol{\tau}_i + \boldsymbol{d}_i(t) - \dot{\boldsymbol{\alpha}}_{Fi} \\ &\quad + \boldsymbol{C}_{F1} \lfloor \boldsymbol{e}_{2i} \rfloor^{\mu_1} + \boldsymbol{C}_{F2} \lfloor \boldsymbol{e}_{2i} \rfloor^{\mu_2}\end{aligned} \tag{50}$$

Using the follower's own fixed-time disturbance observer (FxTDO) to provide disturbance compensation $\boldsymbol{d}_i$, the final formation dynamic control input is given as $\boldsymbol{\tau}_i$:

$$\begin{aligned}\boldsymbol{\tau}_i = \boldsymbol{M}\Big[&-\boldsymbol{f}(\boldsymbol{v}_i) - \boldsymbol{d}_i + \dot{\boldsymbol{\alpha}}_{Fi} - \boldsymbol{C}_{F1} \lfloor \boldsymbol{e}_{2i} \rfloor^{\mu_1} \\ &- \boldsymbol{C}_{F2} \lfloor \boldsymbol{e}_{2i} \rfloor^{\mu_2} - \boldsymbol{\Gamma}_3 \lfloor \boldsymbol{S}_{Fi} \rfloor^{\gamma_3} - \boldsymbol{\Gamma}_4 \lfloor \boldsymbol{S}_{Fi} \rfloor^{\gamma_4}\Big]\end{aligned} \tag{51}$$

Formation stability proof:

Select the candidate Lyapunov function as:

$$V_{Fi} = \frac{1}{2}\boldsymbol{e}_{Fi}^T \boldsymbol{e}_{Fi} + \frac{1}{2}\boldsymbol{S}_{Fi}^T \boldsymbol{S}_{Fi} \tag{52}$$

Taking the derivative yields:

$$\dot{V}_{Fi} = \boldsymbol{e}_{Fi}^T \dot{\boldsymbol{e}}_{Fi} + \boldsymbol{S}_{Fi}^T \dot{\boldsymbol{S}}_{Fi} \tag{53}$$

Substituting Equations (45) and (47) into the first term yields:

$$\boldsymbol{e}_{Fi}^T \dot{\boldsymbol{e}}_{Fi} = \boldsymbol{e}_{Fi}^T(-r_i \boldsymbol{S}_k \boldsymbol{e}_{Fi} + \boldsymbol{e}_{2i} + \boldsymbol{\alpha}_{Fi} - \boldsymbol{R}^T(\psi_i)\dot{\boldsymbol{\eta}}_{di}) \tag{54}$$

where the property of the skew-symmetric matrix $\boldsymbol{e}_{Fi}^T \boldsymbol{S}_k \boldsymbol{e}_{Fi} = 0$ is used. Substituting into Equation (46) yields:

$$\boldsymbol{e}_{Fi}^T \dot{\boldsymbol{e}}_{Fi} = \boldsymbol{e}_{Fi}^T \boldsymbol{e}_{2i} - \boldsymbol{e}_{Fi}^T \boldsymbol{\Gamma}_1 \lfloor \boldsymbol{e}_{Fi} \rfloor^{\gamma_1} - \boldsymbol{e}_{Fi}^T \boldsymbol{\Gamma}_2 \lfloor \boldsymbol{e}_{Fi} \rfloor^{\gamma_2} \tag{55}$$

Substituting the control law (51) into $\dot{\boldsymbol{S}}_{Fi}$, and assuming that the observer has converged, we obtain:

$$\dot{\boldsymbol{S}}_{Fi} = -\boldsymbol{\Gamma}_3 \lfloor \boldsymbol{S}_{Fi} \rfloor^{\gamma_3} - \boldsymbol{\Gamma}_4 \lfloor \boldsymbol{S}_{Fi} \rfloor^{\gamma_4} \tag{56}$$

Combining the terms yields:

$$\begin{aligned}\dot{V}_{Fi} &= \boldsymbol{e}_{Fi}^T \boldsymbol{e}_{2i} - \boldsymbol{e}_{Fi}^T \boldsymbol{\Gamma}_1 \lfloor \boldsymbol{e}_{Fi} \rfloor^{\gamma_1} - \boldsymbol{e}_{Fi}^T \boldsymbol{\Gamma}_2 \lfloor \boldsymbol{e}_{Fi} \rfloor^{\gamma_2} \\ &\quad - \boldsymbol{S}_{Fi}^T \boldsymbol{\Gamma}_3 \lfloor \boldsymbol{S}_{Fi} \rfloor^{\gamma_3} - \boldsymbol{S}_{Fi}^T \boldsymbol{\Gamma}_4 \lfloor \boldsymbol{S}_{Fi} \rfloor^{\gamma_4}\end{aligned} \tag{57}$$

Similarly, during the reaching phase (when the cross term $\boldsymbol{e}_{2i} \to 0$ tends to zero), after arrangement and scaling, we obtain:

$$\begin{aligned}\dot{V}_{Fi} &\le -\lambda_{\min}(\boldsymbol{\Gamma}_1)\| \boldsymbol{e}_{Fi}\|^{\gamma_1+1} - \lambda_{\min}(\boldsymbol{\Gamma}_2)\| \boldsymbol{e}_{Fi}\|^{\gamma_2+1} \\ &\quad -\lambda_{\min}(\boldsymbol{\Gamma}_3)\| \boldsymbol{S}_{Fi}\|^{\gamma_3+1} - \lambda_{\min}(\boldsymbol{\Gamma}_4)\| \boldsymbol{S}_{Fi}\|^{\gamma_4+1}\end{aligned} \tag{58}$$

This can be equivalently transformed into:

$$\dot{V}_{Fi} \le -\mu_1 V_{Fi}^{m_1} - \mu_2 V_{Fi}^{m_2} \tag{59}$$

among them $\mu_1, \mu_2 > 0$; $m_1 = \min(\frac{\gamma_1+1}{2}, \frac{\gamma_3+1}{2}) < 1$, $m_2 = \min(\frac{\gamma_2+1}{2}, \frac{\gamma_4+1}{2}) > 1$。

According to Lemma 1, the error dynamic closed-loop system of each follower strictly satisfies the fixed-time stability theory. This indicates that the multi-AUV formation not only achieves robust tracking against unknown external environmental disturbances, but also ensures that both the formation error and the individual tracking error converge to zero within a fixed time, regardless of how far the initial states deviate. This fundamentally eliminates the long adjustment time inherent in asymptotically convergent control and the high-frequency chattering effects on underwater thrusters caused by traditional sliding mode control.

5 Simulation experiment

To verify the effectiveness and robustness of the proposed algorithm for AUV formation trajectory tracking, simulation studies under different configurations and positions were conducted. The simulation and experimental results show that starting from arbitrary initial configurations,

both the tracking error of each robot and the formation control error can converge to zero within a finite time, the transient response of the system is eliminated, and the formation can stably track the reference trajectory while maintaining the desired configuration. The parameters of the selected AUV model are shown in Table 1. The external disturbances are given as follows.

$$\begin{cases} d_u = 20 + 3*\sin(0.5t) + 3*\cos(0.2t) \\ d_v = 15 + 8*\sin(0.4t) + 4*\cos(0.1t) \\ d_r = 5 + 3*\sin(0.8t) + 2*\cos(0.3t) \end{cases}$$

Tab 1. Model parameters of AUV

Parameter	value	unit
m	185	kg
I_z	50	kg·m^2
X_u	70	kg·s^{-1}
Y_v	100	kg·s^{-1}
N_r	50	kg·m^2·s^{-1}
$X_{\dot{u}}$	-30	kg
$Y_{\dot{v}}$	-80	kg
$N_{\dot{r}}$	-30	kg·m^2
$X_{u\|u\|}$	100	kg·m^{-1}
$Y_{v\|v\|}$	200	kg·m^{-1}
$N_{r\|r\|}$	100	kg·m^2

The control parameters are shown in Table 2, where larger control gain values lead to faster response convergence but also result in higher control inputs, and vice versa. Therefore, reasonable control gains are selected through trial-and-error analysis of the closed-loop system performance and the magnitude of control inputs.

Tab 2. Control parameters

Parameter	Symbol	value	unit
PC distance	a	0.5	m
Kinematic control gain	$k_i(i:1\to3)$	10,10,60	-
Dynamic control gain	$k_i(i:1\to3)$	5,5,5	-
Formation Control Gain	$\beta_i(i:1\to3)$	20,30,10	-
Formation Control Parameter 1	$\rho_i^d(i:1\to2)$	2,2	m
Formation Control Parameter 1	$\phi_i^d(i:1\to2)$	π/2, -π/2	rad
Formation Control Parameter 2	$\rho_i^d(i:1\to5)$	3,2,3,2,2	m
Formation Control Parameter 2	$\phi_i^d(i:1\to5)$	π/2, 3π/4, -π/2, -3π/4, π	rad
Formation Control Parameter 3	$\rho_i^d(i:1\to5)$	3,3,3,3,3	m
Formation Control Parameter 3	$\phi_i^d(i:1\to5)$	2π/5, 4π/5, 6π/5, 8π/5, 2π	rad
Formation Control Parameter 4	$\rho_i^d(i:1\to5)$	3,3,3,3,3	m
Formation Control Parameter 4	$\phi_i^d(i:1\to5)$	5π/3, 11π/6, 13π/6, 7π/3, 2π	rad
Formation Control Parameter 5	$\rho_i^d(i:1\to10)$	2,1,2,1,3,-2,-2,5,-1,-3	m
Formation Control Parameter 5	$\phi_i^d(i:1\to10)$	π/4,π/2,-π/2,-π/4,2π,π/4, -π/4,2π,2π,2π	rad

The reference trajectories for the AUV formation are defined by the equations of $y_d = 10\sin(t/ff)$ and $x_d = t$, with parameter $ff = 8$, and the corresponding results are plotted in Figure 3. The formation tracking errors of the leader and follower AUVs are illustrated in Figures 5 and 5. Figure 4 presents the positional and heading errors of the multi-AUV system. Partial enlarged views distinctly reveal that the Adaptive Sliding Mode Control (ASMC) scheme inherently suffers from chattering and yields relatively slow convergence for certain error curves. In contrast, the proposed algorithm outperforms ASMC in terms of error convergence accuracy, transient performance and

steady-state chattering suppression, delivering higher efficiency and stability for AUV formation tracking control.

Figure 5 depicts the kinematic control inputs of the system. At the initial simulation stage, the velocity commands generated by ASMC suffer from drastic fluctuations, whereas the velocity outputs of the proposed algorithm are smooth and continuous. All velocity components transition steadily toward steady states, enabling smoother control inputs and dynamic responses during AUV formation motion control.

Figure 6 plots the dynamic control input F_u, F_v, τ_r, which characterizes the variation of low-level dynamic control signals. It is observed that the control input curves of ASMC exhibit severe high-frequency oscillation and obvious chattering. By comparison, the control input profiles of the developed algorithm remain much smoother, achieving smoother control outputs and faster transient responses in AUV formation dynamic regulation.

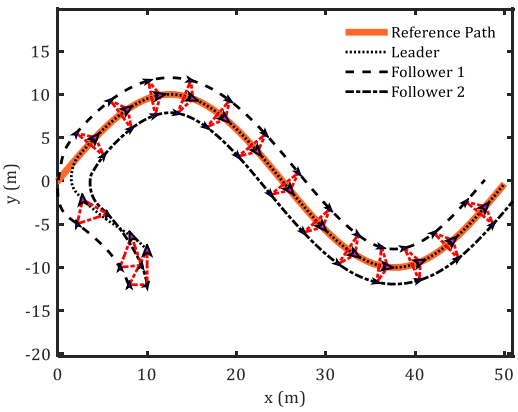

Fig.3. Formation Control of AUVs When Tracking Sinusoidal Reference Paths

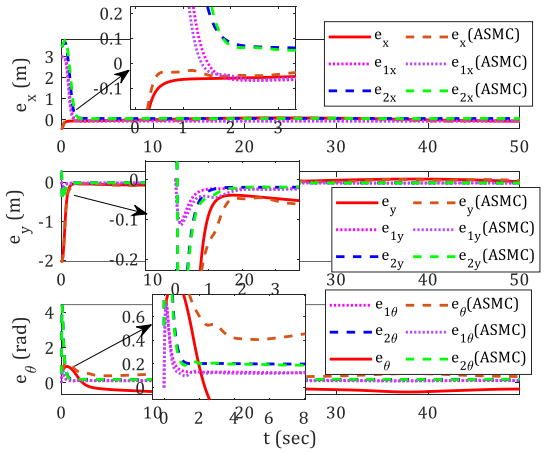

Fig.4. Formation control error signals of AUVs when tracking a sinusoidal reference path

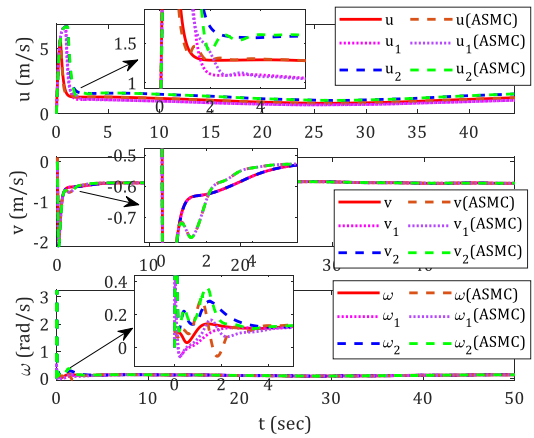

Fig.5. Kinematic control inputs of the leader and

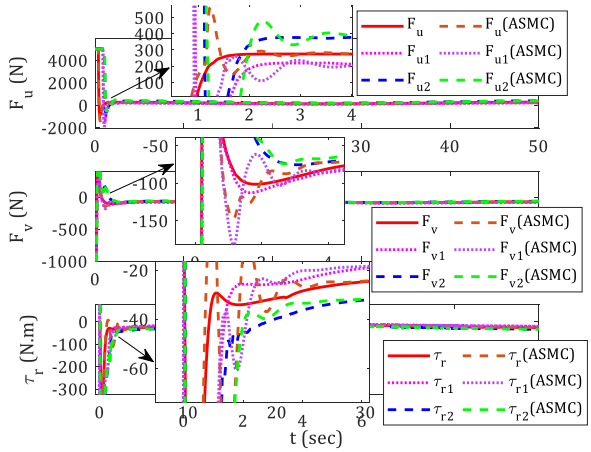

Fig.6. Dynamic control inputs of the leader and follower in AUVs

Figure 7 compares the external disturbances and their corresponding estimated values, where the actual unknown disturbances imposed on AUVs and the estimation outputs of FTDO are plotted separately. As can be seen from the figure, the designed FTDO is capable of accurately and rapidly

estimating time-varying disturbances, and the estimated curve coincides well with the actual disturbance curve, which verifies the effective disturbance capturing capability of the proposed observer against complex perturbations.

Figure 8 shows the temporal evolution of disturbance estimation errors, which intuitively reflects the estimation precision of FTDO. The estimation errors converge rapidly within fixed time and stay within a small neighborhood near zero. The results demonstrate that the developed observer features fast convergence rate and favorable steady-state accuracy.

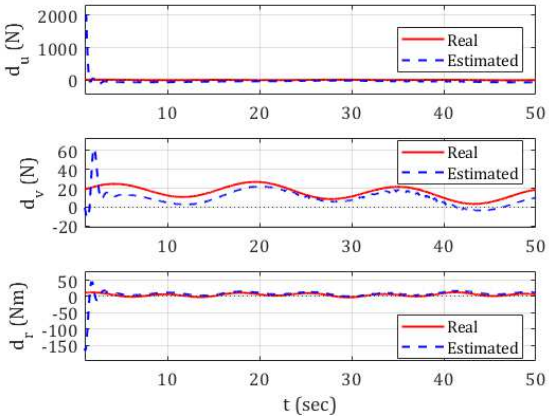

Fig.7 Disturbance and estimation

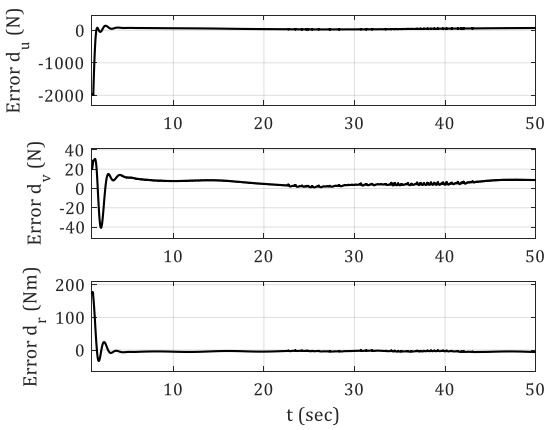

Fig.8 Disturbance estimation error

Formation Control 1: In this formation, one leader and two followers form a triangular formation to perform formation tracking along circular and triangular-circular trajectories. The AUV parameters are shown in Table 2.

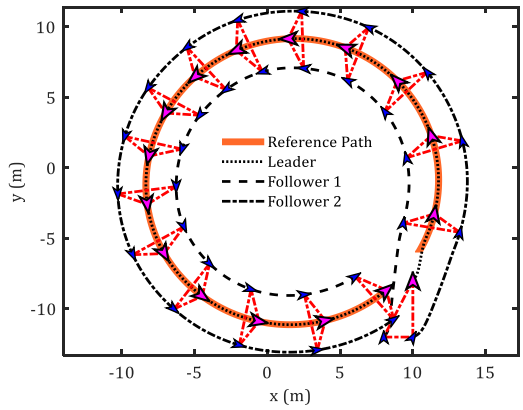

Fig.9. Formation control of AUVs when tracking circular reference paths

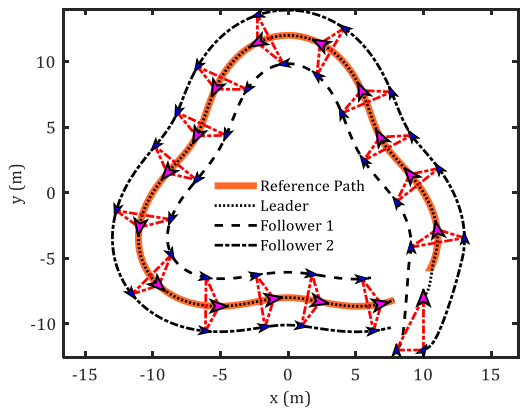

Fig.10. Formation Control for AUVs Tracking a Triangular-Circular Trajectory

Formation Control Case 2: This formation consists of one leader and five followers arranged in a hexagonal configuration to track triangular and quadrilateral circular trajectories, with formation parameters listed in Table 2. As illustrated in Figures 11 and 12, the AUVs start from disparate initial positions either close to or far away from the reference paths, yet all converge to the predefined formation geometry. All AUVs possess distinct initial x and $y=-18$ coordinates and gradually converge to the target formation shape. Figures 11 and 12 verify the control performance under initial large offsets from reference trajectories and the effectiveness of the proposed algorithm with scattered initial positions. In summary, all AUVs can achieve the desired formation within finite time regardless of initial configurations.

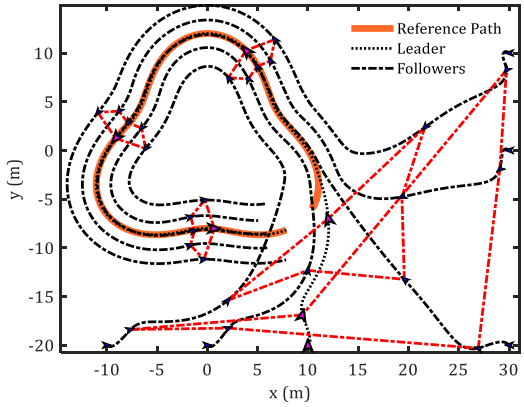

Fig.11. Control of triangular circular path tracking for AUV formations with dispersed initial configurations

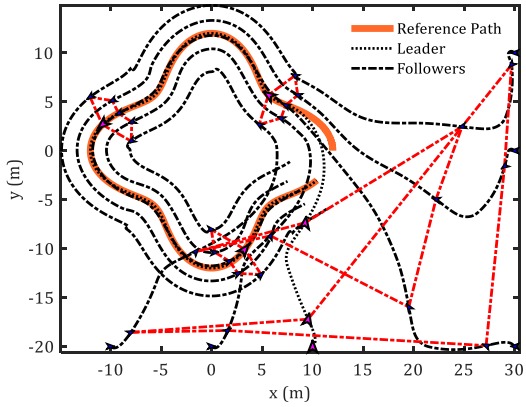

Fig.12. Control of Square-circular path tracking for AUV formations with dispersed initial configurations

Formation Control Case 3: The formation is composed of one leader and five followers configured as a pentagonal formation to track the triangular circular trajectory, where the leader AUV is positioned at the geometric center of the pentagon. Relevant parameters are given in Table 2.

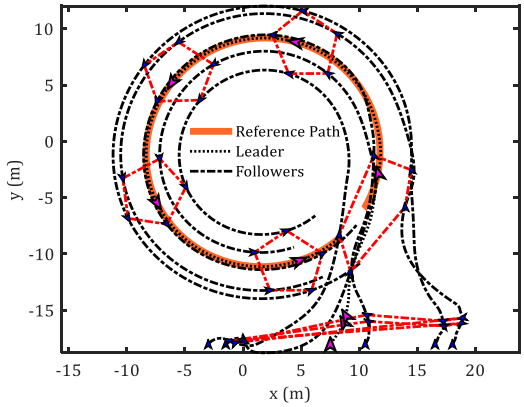

Fig.13. Pentagon Formation Control of AUVs in Tracking Circular Paths

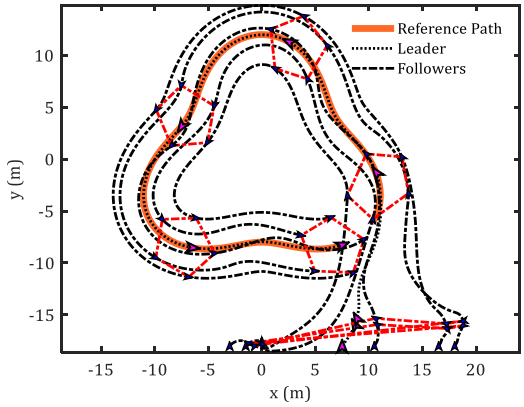

Fig.14. Pentagon Formation Control of AUVs in Tracking Triangular and Circular Paths

Formation Control Case 4: This formation is constructed by one leader and five followers arranged in an arc-shaped configuration to track the quadrilateral circular trajectory, with the leader AUV placed at the rear of the arc. The relevant formation parameters are listed in Table 2.

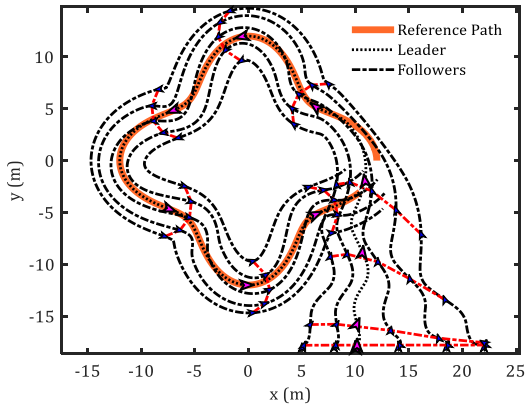

Fig.15. Arched formation control of AUVs when tracking a quadrilateral circular path

Formation Control Case 5: The formation comprises one leader and ten followers arranged in an arrow-shaped configuration to track the circular trajectory, and the leader AUV is located at the center of the formation. The relevant parameters are provided in Table 2.

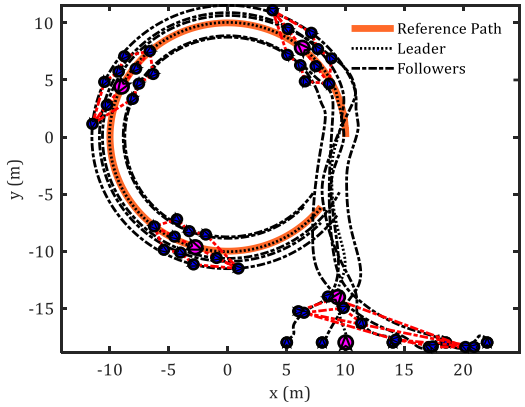

Fig.16. Arrow-shaped formation control of AUVs when tracking a circular path

6 Conclusions

Aiming at unknown ocean current disturbances, model uncertainties and high-precision requirements for real-time cooperative control encountered by multi-AUV formation systems in complicated underwater environments, this paper proposes a robust cooperative trajectory tracking control strategy with fixed-time convergence. Firstly, a Fixed-Time Disturbance Observer (FTDO) is developed to rapidly and precisely estimate internal and external unknown heterogeneous nonlinear disturbances existing in kinematics and dynamics subsystems. Secondly, combining sliding mode theory with the feedforward compensation of the designed observer, a Fixed-Time Sliding Mode Control (FTSMC) law is established. The proposed control scheme improves the anti-disturbance capability of the system and fundamentally suppresses the thruster chattering inherent in conventional sliding mode control. From the perspective of multi-agent coordination, the formation cooperative control law is derived based on the leader–follower framework and angle-distance geometric constraints. Rigorous piecewise Lyapunov stability analysis proves that all state errors of the closed-loop system converge to a small neighborhood around zero within a fixed upper bound of convergence time independent of initial conditions. Finally, numerical simulations under various complex formation configurations (including triangular, hexagonal, pentagonal and arrow-shaped formations) and composite trajectories fully verify the outstanding transient response, steady-state tracking accuracy and strong robustness of the proposed strategy regardless of initial deployment conditions. Future research will further expand to six-degree-of-freedom multi-AUV systems to meet the complex three-dimensional operational requirements in real underwater environments.

Reference list

Shun An, Longjin Wang, Yan He., 2022. Robust fixed-time tracking control for underactuated AUVs based on fixed-time disturbance observer. Ocean Engineering, 266(1), 112567 . DOI: 10.1016/j.oceaneng.2022.112567.

L. P. Fenco Bravo and C. G. Pérez Zuñiga., 2025. Nonlinear trajectory tracking with a 6DOF AUV using an MRAFC controller. in IEEE Latin America Transactions, 23(2): 160-171. DOI: 10.1109/tla.2025.10851362.

Li R, Yang L, Chen Y, Lai G., 2022. Adaptive Sliding Mode Control of Robot Manipulators with System Failures. Mathematics, 10(3): 339. DOI: 10.3390/math10030339.

Hossein M.H. Abdoli, Majdeddin Najafi, Iman Izadi, Farid Sheikholeslam., 2018. Sliding mode approach for formation control of multi-agent systems with unknown nonlinear interactions. ISA Transactions, 80, 65-72. DOI: 10.1016/j.isatra.2018.07.029.

Alireza Hosseinnajad, Mehdi Loueipour., 2022. Fixed-time observer-based homogeneous controller with state-dependent exponent for fault tolerant control of an underwater vehicle. Ocean Engineering, 258, 111737. DOI: 10.1016/j.oceaneng.2022.111737.

Liu Z, Cai W, Zhang M, Lv S., 2022. Improved Integral Sliding Mode Control-Based Attitude Control Design and Experiment for High Maneuverable AUV. Journal of Marine Science and Engineering. 10(6): 795. DOI: 10.3390/jmse10060795.

R. Xu, G. Tang, L. Han, H. Hang and D., Xie. 2019. Robust Finite-Time Attitude Tracking Control of a CMG-Based AUV With Unknown Disturbances and Input Saturation. in IEEE Access, 7, 56409-56422. DOI: 10.1109/access.2019.2914068.

Shou Y, Xu B, Lu H, Zhang A, Mei T., 2022. Finite-time formation control and obstacle avoidance of multi-agent system with application. Int J Robust Nonlinear Control, 32(5): 2883-2901. DOI: 10.1002/rnc.5641.

Zhou Z, Tang G, Xu R, Han L, Cheng M., 2021. A Novel Continuous Nonsingular Finite–Time Control for

Underwater Robot Manipulators. Journal of Marine Science and Engineering. 9(3): 269. DOI: 10.3390/jmse9030269.

Y. Liu, H. Li, R. Lu, Z. Zuo and X. Li. ,2022. An Overview of Finite/Fixed-Time Control and Its Application in Engineering Systems. in IEEE/CAA Journal of Automatica Sinica, 9(12): 2106-2120. DOI: 10.1109/jas.2022.105413.

Rong-Heng Cui, Xue-Jun Xie., 2025. A unifying framework for fixed-time input-to-state stability in stochastic systems. Automatica, 177, 112282. DOI: 10.1016/j.automatica.2025.112282.

Wang Z, Gu Y, Liu J, Zhang Y, Feng K, Dai J, Zheng G., 2025. Event-Triggered Fixed-Time Consensus Tracking Control for Uncertain Nonlinear Multi-Agent Systems with Dead-Zone Input. Actuators. 14(9): 414. DOI: 10.3390/act14090414.

Su, B., Wang, H., Wang, Y. et al., 2021. Fixed-time Formation of AUVs with Disturbance via Event-triggered Control. Int. J. Control Autom. Syst. 19, 1505-1518. DOI: 10.1007/s12555-020-0127-0.

Kaihang Zhang, Wei Zhang, Qiyang Wu, Xue Du. 2025. Adaptive fixed-time disturbance observer-based anti-saturation distributed sliding mode formation tracking control for multi-underactuated AUVs under lumped disturbances. Ocean Engineering, 339(1): 122026. DOI: 10.1016/j.oceaneng.2025.122026.

Shanhai Jin, Yuhan Wang, Dejin Zhao, Xiaodan Wang, Changfu Jin., 2026. Implicit Euler discretization for chattering suppression in non-singular terminal sliding mode control, ISA Transactions, 168: 610-619. DOI: 10.1016/j.isatra.2025.11.022.

An, S.; Wang, X.; Wang, L.; He, Y., 2023. Observer Based Fixed-Time Integral Sliding Mode Tracking Control for Underactuated AUVs via an Event-Triggered Mechanism. Ocean Engineering, 284, 115158. DOI: 10.1016/j.oceaneng.2023.115158.

F. Repoulias and E. Papadopoulos., 2007. Planar trajectory planning and tracking control design for underactuated AUVs. Ocean Engineering. 34(11-12): 1650-1667. DOI: 10.1016/j.oceaneng.2006.11.007.

B. Jiang, Q. Hu and M. I. Friswell.,2016. Fixed-Time Attitude Control for Rigid Spacecraft With Actuator Saturation and Faults, in IEEE Transactions on Control Systems Technology, 24(5): 1892-1898. DOI: 10.1109/tcst.2016.2519838.

A. Polyakov, 2012. Nonlinear Feedback Design for Fixed-Time Stabilization of Linear Control Systems, in IEEE Transactions on Automatic Control, 57(8): 2106-2110. DOI: 10.1109/tac.2011.2179869.

Behera, A. K., & Bandyopadhyay., B. 2016. Event-triggered sliding mode control for a class of nonlinear systems. International Journal of Control, 89(9): 1916-1931. DOI: 10.1080/00207179.2016.1142617.